Energy Transfer Networks Within Upconverting Nanoparticles Are Complex Systems With Collective, Robust, and History-Dependent Dynamics

Ayelet Teitelboim,[‡1] Bining Tian,[‡1,2] David J. Garfield,[1,3] Angel Fernandez-Bravo,[1] Adam C. Gotlin,[1] P. James Schuck,[1,4] Bruce E. Cohen,[1*] and Emory M. Chan[1*]*

The Molecular Foundry, Lawrence Berkeley National Laboratory, Berkeley, CA 94720, USA

[‡] These authors contributed equally to this work.
[*] To whom correspondence should be addressed. E-mail: p.j.schuck@columbia.edu, BECohen@lbl.gov, EMChan@lbl.gov

[1]The Molecular Foundry, Lawrence Berkeley National Laboratory, Berkeley, CA 94720, USA
[2]Department of Physics, Dalian Maritime University, Dalian, Liaoning 116026, China
[3]Department of Chemistry, University of California, Berkeley, CA 94720, USA
[4]Department of Mechanical Engineering, Columbia University, New York, NY 10027, USA

Abstract. Applications of photon upconverting nanoparticles (UCNPs) in biological imaging and solar energy conversion demand that their anti-Stokes luminescence be both tunable and efficient. Rational design of more efficient UCNPs requires an understanding of energy transfer (ET) between their lanthanide dopants – dynamics that are typically characterized by measuring luminescence lifetimes. Existing knowledge, however, cannot explain basic observations in lifetime experiments such as their dependence on excitation power, significantly limiting the generality and reliability of lifetime measurements. Here, we elucidate the origins of the ET dynamics and luminescence lifetimes of Yb^{3+},Er^{3+}-codoped $NaYF_4$ UCNPs using time-resolved luminescence and novel applications of rate equations and stochastic simulations. Experiments and calculations consistently show that, at high concentrations of Er^{3+}, the luminescence lifetimes of UCNPs decrease as much as 6-fold when excitation power densities are increased over six orders of magnitude. Since power-dependent lifetimes cannot be explained by intrinsic relaxation rates of individual transitions, we analyze lifetime data by treating each UCNP as a complex ET network. We find that UCNP ET networks exhibit four distinguishing characteristics of complex systems: collectivity, nonlinear feedback, robustness, and history dependence. We conclude that power-dependent lifetimes are the consequence of thousands of minor relaxation pathways that act collectively to depopulate and repopulate Er^{3+} emitting levels. These ET pathways are dependent on past excitation power because they originate from excited donors and excited acceptors; however, each transition has an unexpectedly small impact on lifetimes due to negative feedback in the network. This robustness is determined by systematically "knocking out," or disabling, ET transitions in kinetic models. Our classification of UCNP ET networks as complex systems explains why UCNP luminescence lifetimes do not match the intrinsic lifetimes of emitting states. In the future, UCNP networks may be engineered to rival the complexity of biological networks that pattern features with unmatched precision.

Introduction

Lanthanide ions in optical materials such as $NaYF_4$:Yb^{3+}/Er^{3+} interact through a network of energy transfer (ET) processes that can aggregate the energy of multiple photons into a single photon of higher energy.[1-3] This phenomenon, known as photon upconversion, has broad utility because it enables the use of near-infrared (NIR) excitation in applications that otherwise require high-energy ultraviolet or visible excitation. NIR light scatters less than shorter wavelengths in heterogeneous media, excites no upconverted autofluorescence, and demonstrates little phototoxicity at the power densities required for upconversion.[4-5] Lanthanide-based colloidal upconverting nanoparticles (UCNPs) do not measurably photobleach even under prolonged single-molecule excitation[4, 6] and have found use in NIR optogenetics,[7-8] photodynamic therapy,[9] cellular imaging,[4] super-resolution imaging,[10-12] and deep-tissue imaging.[5, 11-13] Recently, careful engineering of core-shell UCNP heterostructures has enabled them to be imaged at NIR laser power densities nine or more orders of magnitude lower than with two-photon fluorescence.[13-14] Beyond biological applications, UCNPs have spawned technologies in nanoscale thermometry[15-16] and viscometry,[17] anti-counterfeit labeling,[18] microscale lasers,[19-20] plasmonics,[21] photonic networks,[22] and photovoltaics.[23] Expanding UCNP applications depends largely on increasing upconversion efficiencies, which requires a deeper understanding for how lanthanide excited states dynamically interact.

At a fundamental level, UCNPs are intriguing materials for understanding ET networks on the atomic scale, since each lanthanide dopant ion acts as a node that communicates via ET with the multiple excited states of ions in the same nanoparticle (Figure 1).[24-25] These multi-level systems can upconvert the frequency of incident photons[2] through a series of photophysical transitions that include photon absorption, ET, and radiative decay.[3] Such nonlinear behavior is characteristic of complex ET networks[26] used to facilitate efficient light harvesting in nature[27] and enable optical computation.[28-30] However, the relationship between the topology of upconverting ET networks and their photophysical properties has been difficult to untangle, limiting the ability to engineer optimal application-specific UCNPs.

Excited state dynamics are the critical defining feature of complex systems[31] such as UCNPs and are commonly probed with time-resolved photoluminescence (TRPL) measurements[32-36] to determine key properties such as energy transfer rates, radiative relaxation rates, and quantum efficiency. The lifetimes of TRPL decays are used for applications in multiplexed lifetime imaging,[18] thermometry,[37-38] and binding assays based on ET. Lifetimes are also used to rationalize mechanisms of upconversion,[36] particularly those that enhance[39-41] or quench[33-34, 42] UCNP luminescence. Recent reports,[33, 43] however, suggest that the decay lifetimes of UCNP luminescence may not be reliable indicators of the intrinsic relaxation rates of lanthanide dopants. Indeed, we recently observed that the luminescence lifetimes of UCNPs decrease with the power of their initial excitation.[41] The origins of this power dependence (and history dependence) are unclear, owing to the thousands of photophysical transitions that occur simultaneously in excited UCNPs.[3, 25]

Understanding the mechanisms that give rise to power dependent lifetimes is relevant to biological and photonic applications of upconversion because the powers used to excite UCNPs extend over a broad range,[44] from the low powers (10^{-1} W/cm^2) preferred for imaging cells[4] and live animals[45,13] to the high powers (10^6 W/cm^2) for required for optogenetics,

stimulated emission depletion microscopy,[10-12] and imaging single nanoparticles.[10, 41, 46] Furthermore, systematic benchmarking of transition rates and mechanistic analyses is impossible if routine lifetime measurements are fraught with uncertainty about their underlying meaning and reliability.

Here, we elucidate the origins of the power dependent luminescence lifetimes of Yb^{3+}, Er^{3+}-codoped $NaYF_4$ UCNPs using time-resolved luminescence, deterministic rate equations, stochastic simulations, and data mining of the rates of thousands of parallel transitions. We find that power-dependent lifetimes cannot be explained by intrinsic relaxation rates of individual transitions, so we analyze lifetime data by treating each UCNP as a complex system.[31] This analysis reveals that UCNP emitting states are depopulated more rapidly with increasing excitation power due to ET processes (e.g., ET upconversion and cross relaxation) in which both

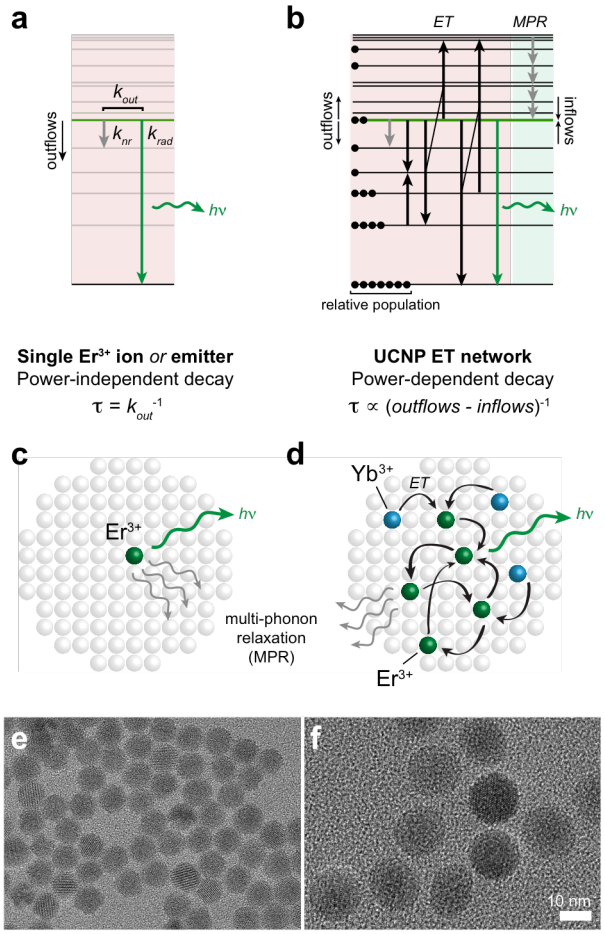

Figure 1. (a) Energy level diagram for the power-independent photoluminescence (PL) decay from an organic fluorophore or an isolated lanthanide ion. Observed lifetimes (τ) of the luminescence from the emitting level (green) are inversely proportional k_{out}, the sum of the radiative (k_{rad}) and non-radiative (k_{nr}) rates of depopulation. (b) Power-dependent decay from a network of lanthanide ions in an upconverting nanoparticle (UCNP). Due to the network of energy transfer (ET) processes, τ is inversely proportional to the difference between the outflows (transitions in red shaded box) and the inflows (green box). (c) Schematic of an isolated lanthanide ion in a lattice (i.e., a single emitter), illustrating its possible relaxation pathways. (d) Schematic of a network of lanthanide ions in a UCNP. (e,f) Transmission electron micrographs of 8-nm core $NaYF_4$: 40% Yb^{3+}, 60% Er^{3+} nanoparticles (e) and core@shell nanoparticles coated with 4 nm $NaYF_4$ (f).

the donor and the acceptor are in excited states, which are heavily populated at high powers. Under these conditions, the decay rate (i.e., the inverse lifetime) is not proportional to the aggregate rate of these depopulating transitions (e.g., Figure 1a), as is commonly assumed.[47-48] Since the ET network rapidly repopulates the emitting level even after excitation is discontinued (Figure 1b), the inverse lifetime is more a consequence of the *difference* between the rates of population and depopulation, which varies with past excitation power.

This work highlights that ET networks in UCNPs are complex systems[31, 49] that exhibit four distinguishing characteristics: collectivity,[50] nonlinear feedback, robustness, and history dependence.[51] At typical excitation powers for UCNPs (10^2-10^6 W/cm^2), the measured luminescence lifetime cannot be interpreted as the average time that an ion spends in an excited state before it relaxes (as in Figure 1c). Rather, the observed lifetimes are the result of energy dissipating through a complex system of photophysical pathways (Figure 1d) in which no single transition determines the observed lifetime. Instead, the component transitions in these complex ET networks act *collectively* and *nonlinearly* to depopulate and repopulate the emitting level. Thus, the scientific relevance of observed luminescence lifetimes can only be extracted in context with historical excitation powers. These results demonstrate that rigorous modeling of lanthanide ET networks as complex systems provides a more accurate understanding of the transient dynamics of UCNPs and other complex ET networks. This understanding will accelerate the development of more efficient UCNPs and enable the precise engineering of ET networks that rival the complexity of biological networks, which are known to pattern features with nanoscale precision.

Methods

Materials. Sodium trifluoroacetate (NaTFA), sodium oleate, ammonium fluoride (NH_4F), lanthanide chlorides (anhydrous, 99.9+%), oleic acid (OA) (90%), and 1-octadecene (ODE) (90%), were purchased from Sigma-Aldrich. $YbCl_3$ hydrate was purchased from Strem.

Synthesis: All syntheses were performed under N_2 flow using standard Schlenk techniques with stirring. The syntheses of the UCNPs core and shells were performed according to previous reports with some modifications.[52]

Synthesis of UCNPs core ($NaY_{0.2}Er_{0.6}Yb_{0.2}F_4$): 32mg of $YbCl_3$ hydrate and 66 mg $ErCl_3$ hydrate were dissolved in 3.25 g OA and 4 mL ODE by heating under vacuum for 1 h at 110 °C. The reaction was cooled to room temperature (RT) under nitrogen flow, followed by the addition of 381 mg sodium oleate, 74 mg NH_4F and 3 mL ODE. The reaction was then heated under vacuum for 20 min, followed by three alternating cycles of refilling with N_2 and purging with vacuum for 1 min per cycle. The reaction temperature was then increased quickly under N_2 to a growth temperature of 315 °C. After 45 min at this temperature, nanocrystal growth was quenched by removing the heating mantle and cooling it with a stream of compressed air, followed by the addition of 20 mL of ethanol and 20 mL acetone at 75°C. The UCNPs were purified twice using ethanol for precipitation and redispersed in hexane with 0.2% (*v/v*) OA. Similar procedures were used for all doped $NaYF_4$ cores.

Preparation of shell precursors. Epitaxial $NaY_{0.8}Gd_{0.2}F_4$ shells were grown on doped $NaYF_4$ cores using a method modified from Li et al.[53] A 0.10 M solution of 80:20 Y/Gd oleate (Y/Gd-OA) was prepared by heating YCl_3 (78 mg) and $GdCl_3$ (26 mg) to 110 °C in oleic acid (2 mL)

and ODE (3 mL) and stirred for 15 min under vacuum. The flask was filled with N_2 and heated to 160 °C for 30 min, followed by another 15 min at 110 °C under vacuum. In a separate flask, a 0.40 M NaTFA-OA precursor solution was prepared by dissolving sodium trifluoroacetate (163 mg) in oleic acid (3 mL) and applying vacuum at room temperature for 20 min.

Synthesis of core/shell $NaEr_xYb_yF_4$ @ $NaY_{0.8}Gd_{0.2}F_4$ *UCNPs:* 27 µmol of purified UCNPs cores in hexane were added to 4 mL of OA and 6 mL ODE. The mixture was degassed for 30 min at 70°C to remove the hexane. The shell growth was performed under N_2 at 280 °C, where alternating injections of Y/Gd-OA and NaTFA-OA precursor were performed at 15 min intervals (see Table S1 in the Supporting Information for volumes). After the last injection the reaction was maintained at 280 °C for additional 30 min to allow for complete shell growth, followed by rapid cooling. Nanoparticles were purified and stored as described for the UCNP cores. Detailed synthesis procedures are given in the Supporting Information.

Sample characterization: All nanocrystals were characterized by powder X-ray diffraction to show pure hexagonal phase**.** TEM images were obtained using a JEOL 2100-F 200 kV field-emission analytical transmission electron microscope.

Optical characterization: UCNP films were drop cast from hexane solutions onto No.1 glass coverslips. Laser scanning confocal imaging was performed in ambient conditions using a custom-built confocal inverted microscope. The sample was excited by a 980 nm continuous-wave laser excitation source (Thorlabs TCLDM9, 300 mW diode) coupled through an oil-immersed objective (100x 1.4NA, Nikon). The emission was collected by the same objective, spectrally filtered using a 514 nm long pass and a 535/30 nm band pass filters and imaged into a free space single-photon avalanche photodiode (SAPD, from MPD). To measure luminescence lifetimes, the laser was operated in a "on-off'' cycle using a function generator, with a square wave with a period of 8 ms. This excitation scheme was implemented to achieve a cycle of 4 ms constant excitation to allow the luminescence to reach steady state, followed by a 4 ms of excitation-free detection of the luminescence decay. The SAPD and the function generator trigger output were collected by a time-correlated-single-photon-counter (PicoHarp 300), enabling photoluminescence transient measurements.

The resulting time-resolved luminescence plots were fit with up to three exponential terms. To quantitatively compare luminescence lifetimes using a single figure of merit, we calculated the effective lifetimes of each trace, τ_{eff}, which is functionally equivalent to the amplitude-weighted average of each lifetime component. This weighted lifetime was calculated by the equation:

$$\tau_{eff} = \frac{\sum A_i \tau_i}{\sum A_i} \qquad (1)$$

Here, τ_{eff} is the weighted lifetime, A_i are weighting factors, and τ_i are lifetimes, obtained from fitting of the decay curve. This expression for τ_{eff} is functionally equivalent to the expression below, which can be calculated from the raw intensity signal, $I(t)$, its maximum I_{max}, and the time t:

$$\tau_{eff} = \frac{\int_{t=0}^{\infty} I(t)}{I_{max}} = \frac{\int_{t=0}^{\infty} \sum A_i e^{-\frac{t}{\tau_i}}}{I(t=0)} \qquad (2)$$

Calculations. *Differential rate equations:* Systems of coupled differential rate equations (DREs) were used to model changes in population for each excited state in the Yb^{3+} and Er^{3+} dopants. Rate equations were assembled automatically using a previously described computational model[25] based on Judd-Ofelt theory[54] and energy transfer models from Kushida.[55] This system of coupled DREs describes the rate at which each lanthanide manifold is populated and depopulated by photon absorption, luminescence, energy transfer, and multiphonon relaxation form its initial steady state population. For a given UCNP composition, rate equations were integrated numerically using Igor Pro 7 (Wavemetrics) to determine the steady state population under a given irradiation power. Then, after discontinuing excitation, the luminescence decay curves and τ_{eff} were calculated using a second round of time-dependent integration. Detailed DRE methods are given in the supporting information.

Kinetic Monte Carlo simulations: A Kinetic Monte Carlo (KMC) model of 8-nm, spherical UCNPs, was implemented in Igor Pro 7 using the rejection-free, Gillespie stochastic simulation algorithm[56] detailed in the Supporting Information. The transition probabilities for each KMC step were calculated using the same rate constants as those used for DREs. Similarly to the DRE calculations, KMC lifetime simulations were performed by discontinuing the excitation after the system reached steady state, i.e., the population of the green-emitting $^4S_{3/2}$ level was recorded over time after the excitation radiation was discontinued. Due to the low population fraction of the $^4S_{3/2}$ level, 10 to 1000 KMC trajectories records were averaged in order to calculate the effective lifetime of each material.

Results and Discussion

Power dependence of UCNP luminescence lifetimes. To investigate the relationship between excitation power and luminescence lifetime of UCNPs, we measured the TRPL of dried films of Yb^{3+}/Er^{3+}-codoped $NaYF_4$ nanocrystals across a range of excitation fluences and doping levels. We synthesized a library of 8-nm-diameter $NaYF_4$ nanocrystals (Figure 1e) with 2, 10, 20, and 60 at% Er^{3+} while keeping the Yb^{3+} concentration constant at 20%. Since quenching at UCNP surfaces shortens luminescence lifetimes,[33-34, 40, 42] we overgrew 4-nm-thick, undoped $NaYF_4$ shells on these nanoparticles (Figure 1f).[53] Representative emission spectra for these UCNPs are shown in Figure S1 in the Supporting Information.

For core and core-shell nanoparticles doped with 20% Yb^{3+} and 2 % Er^{3+}, the decay of the combined luminescence around 518 and 540 nm – corresponding to the Er^{3+}:$^2H_{11/2}/^4S_{3/2}\rightarrow{}^4I_{15/2}$ transitions, respectively – does not vary significantly with excitation power (Figure 2a and Figure 2b; see Figure S2 for lifetimes at 660 nm). However, at higher Er^{3+} doping fractions (20 or 60% Er^{3+}), TRPL traces decay more rapidly as the power is increased, with this power dependence increasing with the Er^{3+} concentration (Figure 2c and Figure 2d). At 20/20% Yb^{3+}/Er^{3+}, the effective lifetime τ_{eff} – defined by Equation 1 in the Methods – decreases by 58% from a maximum of 328±22 μs to 139±3 μs as the excitation power increases from 10^2 to 10^6 W/cm^2 (Figure 3a). At 20/60% Yb^{3+}/Er^{3+}, τ_{eff} decreases six-fold across the same power range, to 62±2 μs. This decrease in luminescence lifetime could be rationalized as the result of the increased depopulation of the emitting state via transitions whose rates are power dependent. Since this dependence is stronger at high Er^{3+}, we hypothesized that these

additional relaxation processes are ET to excited state acceptors.

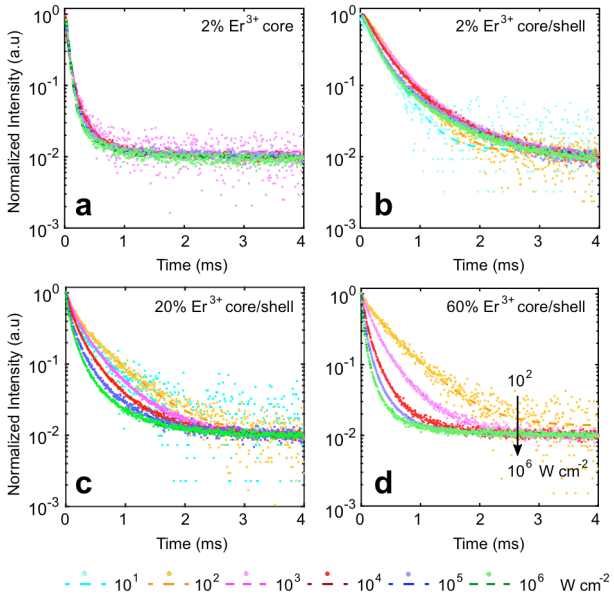

Figure 2. Time-resolved photoluminescence decay traces for the green emission of $NaYF_4$ upconverting nanocrystals excited at 980 nm at six different power densities. All nanocrystals contain 20% Yb^{3+} and are codoped with 2% (a, b), 20% (c) or 60% Er^{3+} (d). Nanocrystals in (a) are 8-nm diameter cores, while nanocrystals in (b), (c) and (d) are 8-nm cores overcoated with 4-nm-thick undoped shells. Emission is filtered between 520-550 nm. Before measuring decays, the luminescence from the samples was allowed to reach steady state during excitation.

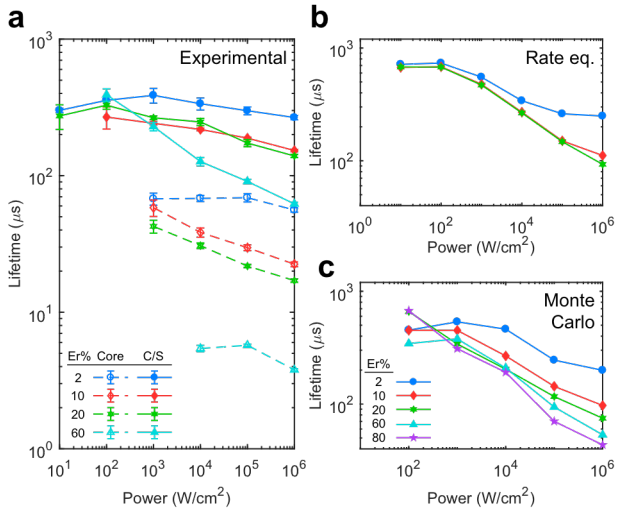

Figure 3. Effective lifetime, τ_{eff}, of the green, Er^{3+}:$^2H_{11/2}/^4S_{3/2} \rightarrow ^4I_{15/2}$ emission vs excitation power measured experimentally for (a) core and core/shell (C/S) $NaYF_4$:20% Yb^{3+}, X% Er^{3+} nanocrystals (X = 2, 10, 20, 60). Error bars depict the 95% confidence limits propagated from uncertainties in exponential fit parameters. τ_{eff} vs excitation power for core-shell nanocrystals calculated using differential rate equations (b) and kinetic Monte Carlo simulations (c).

Calculating luminescence lifetimes. To elucidate the microscopic origins of the power-dependent lifetimes, we used differential rate equations (DREs) to describe the time-dependent changes in population n_i for each excited state *i* in the Yb^{3+} and Er^{3+} dopants. The energy level indices (*i*) used to identify the 36 DREs used in this work are enumerated in Figure 4b and in Table S2 of the Supporting Information. Our computational model[3, 25] automatically constructs and solves systems of coupled DREs that describe the rate $\dot{n}_i = dn_i/dt$ at which each lanthanide $4f^N$ manifold *i* is populated and depopulated by photon absorption, luminescence, ET, and multiphonon relaxation (MPR). To capture the full complexity of these networks, we modeled every interaction – out of thousands of possible combinations of initial and final states – using electric dipole radiative rate constants calculated with Judd-Ofelt theory[54] and energy transfer rate constants using the method of Kushida.[55] Thus, each excited state *i* is a node in the UCNP ET network and is connected to every other state by multiple transitions, each with a distinct rate constant. This DRE treatment is consistent with approaches used to study UCNPs[36] and other complex systems.

Luminescence lifetimes of Yb^{3+}/Er^{3+}-doped UCNPs simulated using DREs exhibited the same qualitative trends as those measured experimentally (Figure 3b; calculated decay curves shown in Figure S3 and S4); τ_{eff} for the 540-nm emission decreased as the power was increased from 10 to 10^6 W/cm^2. Similar to the experimental lifetimes, the simulated power dependence of τ_{eff} increased as the Er^{3+} doping in the Yb^{3+}-codoped UCNPs increased from 2 to 20% Er^{3+}. The qualitative reproduction of the power dependence in the lifetimes suggested that DRE simulations could help elucidate the mechanism for the power dependence of UCNP luminescence lifetimes.

For UCNPs doped above 20% Yb^{3+} or 20% Er^{3+}, numerical integration of the DREs does not converge with respect to reduction in the time step due to rapid energy transfer between closely spaced dopants. Therefore, we calculated the luminescence decays of materials with high dopant compositions using Kinetic Monte Carlo[43, 56-58] (KMC) simulations of 8-nm spheres with randomly distributed lanthanide ions (Figure S5; see KMC methods in Methods section). Luminescence lifetimes simulated via KMC (Figure 3c) exhibited similar power dependence to those observed experimentally and to those calculated with DREs. Specifically, τ_{eff} values decreased with power, with the power dependence increasing as the Er^{3+} content increased from 20% to 80%.

The luminescence lifetime of an ET network is much longer than the lifetime of an excited ion in the network. To uncover the pathways that give rise to power dependent behavior, we mined the DRE results by isolating the specific transitions that populate and depopulate the Er^{3+}:$^4S_{3/2}$ level, which emits 540-nm photons. Since the luminescence lifetime of a simple emitter is proportional to the rate that an emitting level is depopulated (as in Figure 1a), we filtered the DRE data for all transitions that originate from the $^4S_{3/2}$ manifold. We calculated the rates of these transitions using their rate constants and the populations of their initial states. Since transition rates vary over time as the excited state populations decay (as in Figure S8), we sought to measure those rates at a time at which the transition rates were characteristic of the effective luminescence lifetime of the decaying system. We postulated that this occurs at t_{eq}, which we define as the "equivalent time" at which the relative rate of change in the population $\bar{n}_i$ of the emitting level *i*, equals the inverse lifetime (i.e., $\bar{n}_7(t_{eq}) = \dot{n}_7(t_{eq})/$

$\dot{n}_7(t_{eq}) = -\tau_{eff}^{-1}$, where $\dot{n}_7 = \frac{dn_7}{dt}$, and index 7 refers to the Er^{3+}:$^4S_{3/2}$ manifold). All reported transition rates reported below were calculated at t_{eq}, which can be visualized on plots of $\bar{\dot{n}}_7(t_{eq})\ vs.\ t$ in Figure S8 and S9. Additional details of t_{eq} usage are given in Section 2 of the Supporting Information.

For 20/20% Yb^{3+}/Er^{3+}-doped UCNPs excited at 10^6 W/cm^2, data mining reveals that over 1700 different photophysical transitions depopulate the Er^{3+}:$^4S_{3/2}$ manifold. The aggregate rate of these outflows, normalized by the $^4S_{3/2}$ population, was $\bar{\dot{n}}_{7,out}$ = 77,000 s^{-1} at t_{eq} = 110 µs (Figure 4a). In this work, we occasionally refer to depopulating and populating transitions as *outflows* and *inflows*, respectively, for brevity and to avoid confusion between the multiple meanings of the word *population*. To account for 95% of the outflow rate, one must aggregate the rates of the 45 fastest depopulating transitions, listed in Table S7 in the Supporting Information. In fact, the five most significant outflows account for only 53% of the aggregate outflow rate. The remaining 42% require contributions from 40 more transitions. Thus, at high excitation powers, the depopulation of a lanthanide excited state cannot be attributed to a single pathway or to even a few major transitions. Instead, many minor transitions act *collectively* to depopulate the $^4S_{3/2}$ manifold. Collective behavior – in which interactions between species in a network produce coordinated activity distinct from that of isolated species – is notable since it is a defining trait of complex systems.[31, 49-50]

For a simple emitter (as in Fig. 1a), the inverse of the relative rate, $1/\bar{\dot{n}}_{7,out}$, should equal the luminescence lifetime.[47] However, for 20/20% Yb^{3+}/Er^{3+}-doped nanocrystals excited at 10^6 W/cm^2, this theoretical lifetime, $1/\bar{\dot{n}}_{7,out}(t_{eq})$ = 13 µs, is seven-fold lower than the τ_{eff} = 93 µs calculated from the decay curves of the simulation (i.e. $n_7(t)$). This disparity between $\bar{\dot{n}}_{7,out}$ and τ_{eff}^{-1} further suggests that the power dependence of τ_{eff} is a consequence of a mechanism more complex than that of a traditional emitter.

To explain why the luminescence from a lanthanide manifold can persist for so long, we reasoned that for a complex system, the decay dynamics are not solely determined by relaxation rates since inflows can increase the population of an emitting level (as shown in Figure S8, the inflow rate is significant throughout the decay transient). Thus, the overall rate of change in an excited state population, $\dot{n}$, would be the sum of all rates of transitions that depopulate and populate that species, $\dot{n}_{net} = \dot{n}_{in} + \dot{n}_{out}$. Here, $\dot{n}_{in}$ is the aggregate inflow

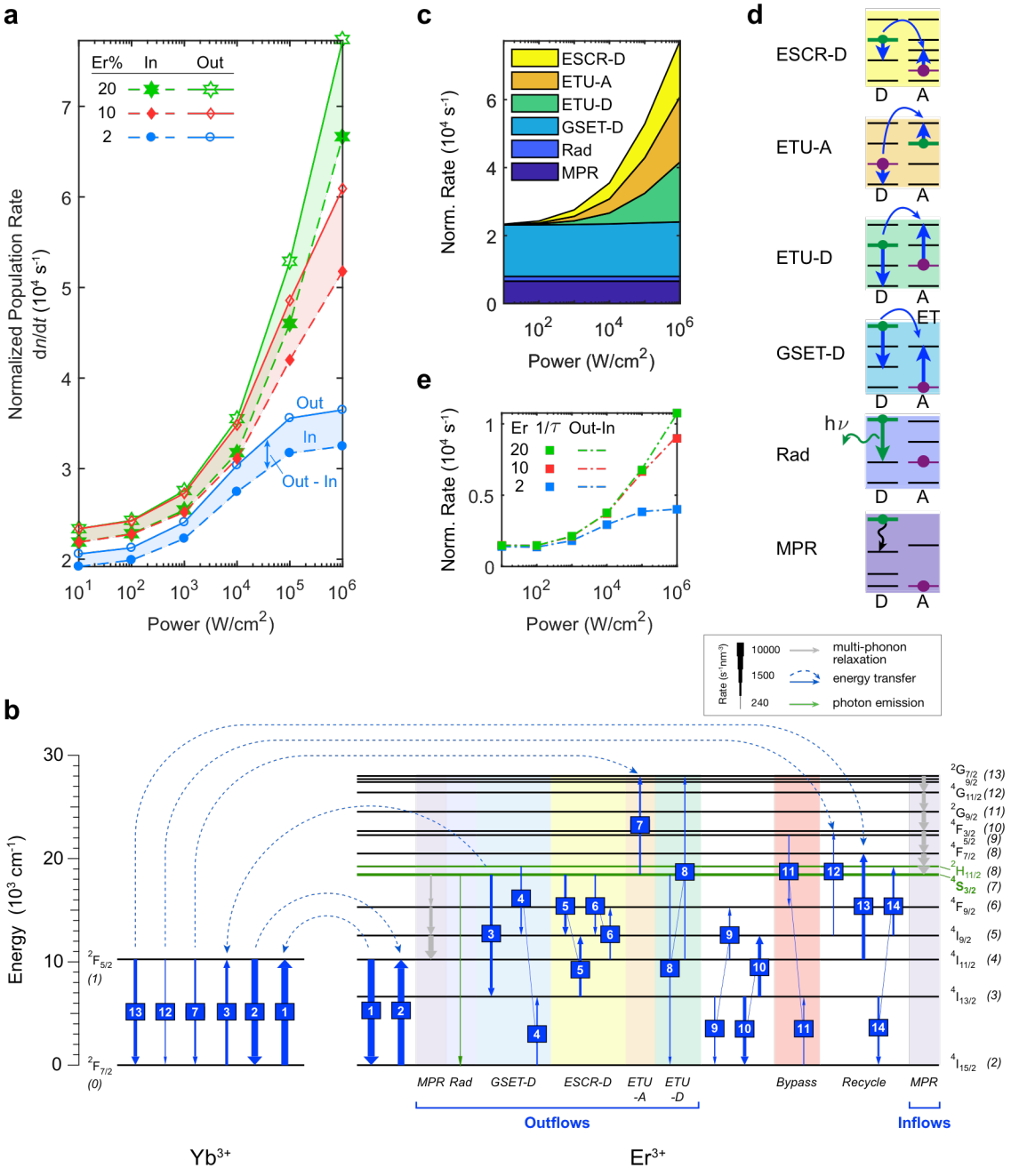

Figure 4. (a) Comparison of the outflow and inflow rates for the emitting Er^{3+}:$^4S_{3/2}$ level for 20% Yb^{3+}/ X% Er^{3+}-doped UCNPs doped at three Er^{3+} concentrations (X = 2, 10, 20%) and excited at six powers. Aggregate, population-normalized rates of transitions that populate (dashed lines) and depopulate (solid lines) the emitting level are calculated using rate equation models; data is shown for time t_{eq}. Shaded regions highlight differences between outflow and inflow rates for each composition. (b) Major transitions for 20/20% Yb^{3+}/Er^{3+}-doped UCNPs excited at 10^6 W/cm^2 calculated at t_{eq} = 110 μs. Arrow thicknesses scale logarithmically with rates. Manifolds are labeled by their $^{2S+1}L_J$ term symbols and their index *i* (italics) used for rate equation analysis. (c) Stack plot of contributions from the six transition classes, defined in (d), to the population-normalized rate of outflows from the $^4S_{3/2}$ manifold. The emitting level (green lines) can act as either a donor (D) or acceptor (A). Circles denote dopant ions occupying given states. (e) Power dependence of the $1/\tau_{eff}$ (symbols) and the difference between outflow and inflow rates at t_{eq} (lines, see text for definitions).

rate, and the outflow rate $\dot{n}_{out}$ is negative to reflect a decrease in the population. For a luminescent decay, we postulated that ${\tau_{eff}}^{-1} \approx \bar{\dot{n}}_{net} = |\bar{\dot{n}}_{out}| - |\bar{\dot{n}}_{in}|$ at a time characteristic of the decay. For a simple emitter (e.g., an isolated lanthanide ion), $\bar{\dot{n}}_{in} \approx 0$ during the decay due to the absence of excitation, leading to the traditional inverse relationship between τ_{eff} and $\bar{\dot{n}}_{out}$. In contrast, for a UCNP ET network, an emitting manifold in principle can continue to be populated after excitation is discontinued, via relaxation from higher lying manifolds and via energy transfer from excited ions nearby. In this case, $\bar{\dot{n}}_{in} \neq 0$ for UCNPs with high excited state populations, thereby explaining the discrepancy between $1/\bar{\dot{n}}_{7,out}$ and τ_{eff}, especially for high doping levels that foster rapid ET between ions.

To investigate the role of inflows on lifetimes, we mined the DRE results for transitions that populate the $^4S_{3/2}$ manifold in 20/20% Yb^{3+}/Er^{3+}-doped nanocrystals excited at six different powers. At high excitation power (10^6 W/cm^2), the aggregate rate of inflows populating the $^4S_{3/2}$ level is significant as suspected – reaching 86% of the aggregate outflow rate (Figure 4a) as calculated at t_{eq}. Even at lower Er^{3+} concentrations (i.e., 2% and 10% Er^{3+}), $\bar{\dot{n}}_{7,in}$ is still a significant fraction of $\bar{\dot{n}}_{7,out}$ at 10^6 W/cm^2 (Figure 4a).

Due to the significance of $\bar{\dot{n}}_{7,in}$ at high powers and high Er^{3+} doping, the *overall* rate of change in the population ($\bar{\dot{n}}_7 = |\bar{\dot{n}}_{7,in}| - |\bar{\dot{n}}_{7,out}|$) is only 16% of $\bar{\dot{n}}_{7,out}$ for 20/20% excited at 10^6 W/cm^2, explaining why τ_{eff} is 7-fold longer than $1/\bar{\dot{n}}_{7,out}$ at high excitation power. As postulated, after accounting for both inflows and outflows, the inverse lifetime $1/\tau_{eff}$ is identical to $\bar{\dot{n}}_7$ at all powers and all Er^{3+} doping levels, as shown in Figure 4e. This equality was predetermined by our definition of t_{eq}; however, this self-consistency validates our assumption that the microscopic dynamics of thousands of transitions at t_{eq} are reflective of a decaying system with τ_{eff}.

An important consequence of the dependence of the luminescence lifetime on inflow transitions is that the measured luminescence lifetime of a UCNP is not an accurate reflection of the dynamics of individual excited states inside the UCNP ET network. Monte Carlo simulations illustrate that the number of Er^{3+} ions in a UCNP in their $^4S_{3/2}$ state fluctuates much more rapidly than the luminescence decay rate from that state (Figure S6). Depopulating transitions transiently reduce the $^4S_{3/2}$ population (occasionally to zero), but subsequent ET processes can quickly repopulate the emitting level. To illustrate the atomistic origins of this behavior, we tracked the elapsed time, τ_{traj}, between the promotion or demotion of an ion to an Er^{3+}:$^4S_{3/2}$ state and the time when the energy of that individual state is consumed in whole or in part for another transition (e.g., photon emission or non-resonant energy transfer, which may occur on a different ion due to resonant energy migration). A graphical illustration of the derivation of τ_{traj} is shown in Figure S7a. The average value of τ_{traj} calculated for UCNPs doped with 20% Yb^{3+} and 20% Er^{3+} (7.8 μs at 10^6 W/cm^2, see histogram of lifetimes in Figure S7b) is an order of magnitude smaller than τ_{eff} (75 μs). Thus, the lifetime of an individual excited state trajectory (τ_{traj}) is significantly shorter than the luminescence lifetime. The "birth" of new energy trajectories via populating transitions partially offsets the rapid "death" of trajectories via depopulating transitions. Therefore, the ET network decays as a system rather than a collection of isolated dopant ions. The stark contrast between the dynamics of the network and the dynamics of individual dopant states is a second characteristic of complex systems.

The overall, relative rate determines the power dependence of the luminescence

lifetime. Using the population balance model above, we reasoned that variations in the overall rate $\bar{\dot{n}}_7$ (normalized by population) could explain the power dependence of luminescence lifetimes. Indeed, as the excitation power is increased above 10^3 W/cm^2 for DRE-simulated 20/20% Yb^{3+}/Er^{3+} UCNPs, the magnitude of $\bar{\dot{n}}_7$ increases dramatically (Figure 4e). This overall rate (relative outflows minus relative inflows) is seven-fold greater at 10^6 W/cm^2 than at 10 W/cm^2, resulting in a corresponding, seven-fold decrease in τ_{eff} at the higher power. Notably, $\bar{\dot{n}}_{7,in}$ and $\bar{\dot{n}}_{7,out}$ both increase with power (Figure 4a), which is intuitive since the rates of ET inflows and outflows increase as excited state populations increase. Thus, it is the power dependence of the *difference* in these relative rates that is key to explaining the power-dependent lifetimes.

Microscopic origins of power-dependent population and depopulation. To uncover the microscopic pathways that give rise to the power dependence of τ_{eff}, we investigated the individual transitions that populate and depopulate the green-emitting Er^{3+} transition in Yb^{3+}-codoped UCNPs. As shown in the mechanism in Figure 4b in the "Inflows" category and in Tables S6 and S7, the green-emitting $^4S_{3/2}$ and $^2H_{11/2}$ manifolds are *populated* predominantly by MPR from the Er^{3+}:$^4F_{7/2}$ manifold. The $^4F_{7/2}$ level is itself populated mostly via MPR from higher lying manifolds. However, the $^4F_{7/2}$ level and other higher lying manifolds can also be populated via power-dependent energy transfer upconversion (ETU) from other excited states (e.g., "recycling" transitions 12-14 in Figure 4b), which are themselves populated via multiple pathways. Furthermore, excited states higher in energy than the emitting level can be depopulated by cross-relaxation, allowing upconverted energy to bypass the emitting level (e.g., transition 11 in Figure 4b). Thus, it is challenging to attribute the population of the $^4S_{3/2}$ emitting level to a single pathway beyond the most immediate MPR transition, which has no intrinsic power dependence.

To analyze the transitions that *depopulate* the green-emitting levels, we categorized these transitions into the six classes defined below. We distinguished ET classes by their effect on the excited state populations above and below the emitting level – which we hypothesized would influence the power dependence of luminescence lifetimes.

1. Energy Transfer to a Ground State Acceptor (GSET-D). The depopulating transition with the largest rate is the back transfer of energy from Er^{3+} to Yb^{3+} (ET arrow pair 3 in Figure 4b). The total branching ratio β for this transition is 15% at 10^6 W/cm^2, where β is defined mathematically[25] in Section 2 of the Supporting Information. The Er^{3+}:$^4S_{3/2}$ emitting state is the donor, while the acceptor is the Yb^{3+} ground state. Since the large Yb^{3+} ground state population, n_0, is reasonably invariant, the relative rate of this transition should not change significantly with power. This lack of power dependence applies more generally to all ET transitions that involve a ground state acceptor – a class we term "Ground State Energy Transfer-Donor" (GSET-D) and show schematically in Figure 4d. We tested this hypothesis by calculating $\bar{\dot{n}}_{7,GSET}$, the sum of the normalized rates of all GSET-D transitions originating from the green-emitting level. As expected, $\bar{\dot{n}}_{7,GSET}$ does not vary appreciably with power at 20% Er^{3+} (Figure 4c) or lower concentrations (Figure S10 and S11, Supporting Information).

2 & 3. Radiative and multi-phonon relaxation. Similar analysis reveals that the normalized rates of radiative relaxation and MPR do not exhibit power dependence (Figure 4c).

4. Excited State Cross Relaxation Donor (ESCR-D). The transition with the second-highest

branching ratio from Er^{3+}:$^4S_{3/2}$ is ET to an Er^{3+}:$^4I_{13/2}$ acceptor (ET transition 5 in Figure 4b). This transition belongs to a class characterized by the emitting state acting as a donor for cross-relaxation (CR) transitions in which the acceptor is an excited state (ESCR-D, Figure 4d). We define cross-relaxation as an ET process that results in the donor and acceptor having final states that lie between the initial energies of the two ions. Unlike GSET-D transitions, ESCR-D transitions exhibit a strong power dependence (Figure 4c), which is not surprising since ESCR-D rates are proportional to the product of the populations of the donor (n_d) and acceptor levels (n_a). Both populations are highly dependent on excitation power, and normalizing the rates by the Er^{3+}:$^4S_{3/2}$ population removes only the dependence on n_d (see Equation S9 in the Supporting Information).

5. Energy Transfer Upconversion Acceptor (ETU-A). In this transition class, the emitting level acts as an acceptor for energy transfer upconversion (ETU-A, Figure 4d), with the archetype being ET transition 7 in Figure 4b. The normalized ETU-A rate exhibits a strong dependence on the excitation power (Figure 4c), growing from a non-existent contribution at 10 W/cm^2 to 21% of the total $^4S_{3/2}$ depopulation rate excited at 10^6 W/cm^2 in 20/20% Yb^{3+}/Er^{3+} UCNPs.

6. Energy Transfer Upconversion Donor (ETU-D). Here, the emitting state is the ETU *donor* (Figure 4d), with the most significant example being ET transition 8 in Figure 4b. Like the ETU-A rate, $\bar{\dot{n}}_{7,ETU-D}$ is highly power-dependent (Figure 4c), with its contribution growing to 23% of the overall depopulation at 10^6 W/cm^2.

Among the six classes of outflows discussed above, the most significant contributors to the power dependence of $\bar{\dot{n}}_{7,out}$ are ESCR-D, ETU-A, and ETU-D. Interestingly, these three transition classes contribute relatively equally to the increase in the depopulation rate as the excitation power is increased (Figure 4c) – further supporting our conclusion that the power dependence of τ_{eff} is a consequence of the collective behavior of UCNP ET networks. Although it is tempting to conclude that ETU-A, ETU-D, and ESCR-D are the major pathways for shortening UCNP luminescence lifetimes at high power, we recall that $1/\tau_{eff}$ is proportional to the *difference* between $\bar{\dot{n}}_{7,in}$ and $\bar{\dot{n}}_{7,out}$, requiring us to account for inflows as well. The power dependences of inflows are difficult to rationalize because many convergent pathways supply a given inflow. Likewise, depopulating transitions may branch out and feed back into the emitting level to repopulate it, dampening any effect on the *overall* rate. Thus, due to the complexity of ET networks, we needed to extend our analysis with a second approach to quantify the contributions of the different transition classes to the power dependence of luminescence lifetimes in UCNPs.

Knocking out transitions confirms collective network behavior. To determine the extent to which each transition type contributes to decreasing luminescence lifetimes in lanthanide-doped upconverting materials, we postulated that *deactivating* the transitions responsible for decreasing the lifetimes at high powers would result in recovery of the lifetimes back to their low-power values. Conversely, disabling "unimportant" transitions would not alter the lifetime significantly. Similar to gene knockout experiments used to study complex regulatory networks in organisms,[59] transition knockouts allow us to investigate the function of

each transition type in an ET network as UCNP luminescence decays. To implement this strategy, we modified our DRE calculations to disregard all transitions of a specified type originating from the emitting state during the TRPL decay (but not during excitation. See Supplemental Methods for additional details).

Knocking out individual classes. To begin, we knocked out the transitions in each of the four classes – GSET-D, ESCR-D, ETU-D, and ETU-A – that exhibited the largest contributions to the power-dependent depopulation of the Er^{3+}:$^4S_{3/2}$ manifold (as illustrated in Figure 4c). When GSET-D transitions from the $^4S_{3/2}$ manifold are deactivated in 20/20% Yb^{3+}/Er^{3+} UCNPs excited at 10^6 W/cm^2, the calculated τ_{eff} for the Er^{3+}:$^4S_{3/2}\rightarrow{}^4I_{15/2}$ luminescence increases marginally from 93 to 122 µs (Figure 5). When ETU-D transitions are knocked out, τ_{eff} does not change significantly. In general, none of four, single-knockout experiments resulted in luminescence lifetimes that were as long as the low-power lifetime of 679 µs at 10 W/cm^2 (Figure 5). This result reaffirms our observation that no single class of transitions is solely responsible for decreasing the luminescence lifetime in UCNPs. The insensitivity of τ_{eff} to the removal of major depopulating transitions is a consequence of the many ET pathways through which energy flows out of the emitting manifold. When a single depopulation pathway is blocked, energy flows divert to alternate depopulation pathways, resulting in a significantly smaller effect on τ_{eff} than expected. Thus, the net change in the normalized rate, $1/\tau_{eff}$, is damped. This robustness towards perturbation is a third characteristic that UCNP ET networks share with complex systems.

Double and triple knockouts. To test whether multiple transitions act cooperatively to reduce luminescence lifetimes, we simultaneously knocked out pairs of the four transition classes. As with the single knockouts, eliminating pairs of these classes only slightly increased τ_{eff} for the green-emitting level (Figure 5). The largest lifetime achieved after double knockouts is ca. 140 µs for the GSET-D/ETU-A pair and for the GSET-D/ESCR-D pair – significantly shorter than the low-power target of 679 µs. When we simultaneously knock out three transition

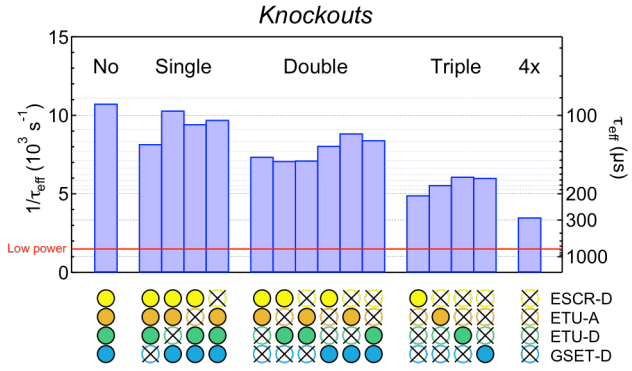

Figure 5. Transition knockout calculations. Change in effective lifetime τ_{eff} after simultaneously knocking out combinations of 1, 2, 3, and 4 different transition classes from rate equation calculations. Knockout combinations were formed from the four major classes of transitions (ESCR-D, ETU-A, ETU-D, and GSET-D) that originate from the emitting Er^{3+}:$^4S_{3/2}$ manifold in 20/20% Yb^{3+}/Er^{3+}-doped UCNPs excited at 10^6 W/cm^2 power density. Hollow, crossed-out circles (⊗) mark the color-labeled transition classes that are knocked out. Filled circles (●) denote transition classes that are still active. The red line indicates τ_{eff} calculated at 10 W/cm^2 and represents the idealized target (i.e., knockout of all processes that contribute to the power dependence of the lifetime).

classes (Figure 5), more substantial increases in the lifetimes are observed compared to pairwise knockouts, with the largest increase (to 203 μs) observed when knocking out ETU-A, ETU-D, and GSET-D transitions simultaneously. Surprisingly, the low-power lifetime is still not recovered even when three out of the four major classes of outflows are disabled.

Quadruple knockout. Finally, we deactivated all four of the major transition types simultaneously. Without these transitions, τ_{eff} increased to 285 μs – which was the most significant increase in lifetime of all of the knockout experiments. It is surprising that we still only recover 42% of the low-power lifetime of 679 μs even after knocking out all four major sources of depopulation. The discrepancy may arise from the fact that the low power decays originate from initial excited state populations that are orders of magnitude lower than the high-power knockout experiments. Full recovery of low-power lifetimes might be achieved by knocking out power-dependent transitions other than those that originate from the $^4S_{3/2}$ manifold.

The insensitivity of the lifetime to knockouts could alternately be explained by a two-step chain reaction model ($A \xrightarrow{k_{\text{in}}} B \xrightarrow{k_{\text{out}}} C$), in which species *B* is the emitter (*i* = 7), *A* is a reservoir state that populates *B* (i.e., the Yb^{3+} excited state), and k_{in} and k_{out} are rate constants. When $k_{in} << k_{out}$, then the first step is the rate limiting step, and the dynamics of *B* are dominated by k_{in}. If this mechanism applied to the lanthanide ET networks in this work, their luminescence lifetimes would be less sensitive to knockouts of outflow transitions until the aggregate outflow rates were reduced to the point where they were comparable with inflow rates (see SI Section 10 for detailed explanation). However, we do not believe that this simple chain mechanism accurately models the complexity of lanthanide ET networks. Unlike the chain model, the calculated outflow and inflow rates are comparable in magnitude, with $|\bar{\dot{n}}_{out}/\bar{\dot{n}}_{in}|$ never exceeding 1.2 (Figure 3 and Figure S15). In addition, lifetimes and decay traces of the Yb^{3+}:$^2F_{5/2}$ state show distinct dynamics from the Er^{3+}:$^4S_{3/2}$ state (Figure S4), even though similar dynamics are predicted by the simple model. This discrepancy is understandable, since the convoluted and non-linear ET interactions are not captured by the linear chain mechanism. Thus, we believe that the network robustness is a function of the complexity of the ET network rather than the dominance of a single, rate-limiting step.

The fact that we need to simultaneously knock out all four transition types to achieve maximum lifetime recovery indicates that each of these classes play a role in the cycle of depopulation and re-population of the emitting state. To determine if the contributions of each class are strictly additive or if the transitions interact synergistically, we constructed a matrix-based model that takes into account all 2, 3, and 4-way interactions between the classes (i.e., those involving 2, 3, or 4 classes), as described by Equation S10 and Figure S12 in the Supporting Information. We solved Equation S10 using the knockout data to quantify the contributions from each interaction type to τ_{eff}^{-1}. As shown in Figure S13, 20/20% Yb^{3+}/Er^{3+} UCNPs excited at 10^6 W/cm^2 exhibit strong individual contributions (>3000 s^{-1}) to τ_{eff}^{-1} from the GSET-D, ETU-D, and ETU-A transition classes, in order of decreasing significance. Several higher-order interactions, particularly the ETU-A/GSET-D pairwise interaction and the 4-way interaction, have substantial positive contributions to τ_{eff}^{-1}, indicating synergism between these transition classes beyond the sum of their individual contributions. All of the 3-way interactions and three pairwise interactions have negative contributions, suggesting that ET transitions can

inhibit each other. The significance of these 2, 3, and 4-way interactions demonstrates that ET interactions in UCNPs are highly non-linear, with positive and negative feedback loops that are characteristic for a photophysical network with such complex topology.

The strong contributions of high-order interactions further support our conclusion that all four major classes of depopulating transitions (GSET-D, ETU-D, ESCR-D, and ETU-A) act *collectively* and not independently to shorten the lifetime of UCNP luminescence excited at high power. Even the GSET-D transitions, whose rates do not vary with power, are required. Thus, *all* of the interactions are required to accurately model the power dependence of the lifetime. These models inform our final description of the UCNP luminescence decays in which the energy stored in dopant excited states unwinds nonlinearly over time through a complex system of GSET-D, ETU-D, ESCR-D, and ETU-A transitions. The power dependence of luminescent lifetimes thus originates from the dependence of these networks on the excited state populations at the start of the decay, which are determined by the power of the discontinued excitation source. This history dependence, while expected for a non-equilibrium process, is the fourth and final characteristic of complex systems that we observed in UCNPs.

Conclusions

In this work, we elucidate the collective decay mechanism that gives rise to the power dependence of luminescence lifetimes of UCNPs. We conclude that ET networks are complex systems because they exhibit four defining characteristics:[51] non-linear feedback,[30, 60] collectivity,[50] robustness towards perturbation,[27] and history dependence. These traits shape the power-dependence of UCNP luminescence lifetimes because Er^{3+} emitting states are depopulated and repopulated at high power through the collective action of many seemingly minor ET processes, rather than through a single dominant pathway. The complexity of these ET networks results in nonlinear responses in the lifetime due to positive and negative feedback in the network. This non-linearity and robustness were established and characterized by systematically knocking out combinations of ET transition classes. Finally, UCNP luminescence lifetimes are history-dependent because the excitation power sets the initial populations of all excited states, thereby determining ET rates, particularly those between pairs of excited states, long after excitation is discontinued. These results highlight that UCNP ET networks are complex systems with lifetimes dramatically different that those of their components, i.e., excited dopants in the network.

The results presented here should stimulate further work on the dynamics of UCNP ET networks and their applications. The transition classification and knockout scheme will be essential for engineering UCNP lifetimes and energy transfer. Our calculations demonstrate that since lanthanide ET networks are highly convoluted and nonlinear, knocking out small number of outflow transitions does not result in a significant change in the lifetime, highlighting the importance of inflows in lanthanide decay dynamics. In the future, experimental techniques for knocking out power dependent transitions will be combined with our computational knockout approaches to further explore and manipulate the power dependent dynamics in UCNPs.

Finally, this work has several key implications for researchers of upconversion and other complex ET networks:

1. *Using decay lifetimes to measure transition rates in complex systems is not straightforward*, particularly at the high excitation powers typically used to image single UCNPs. This work demonstrates how the photophysical dynamics of lanthanide excited states in UCNPs, and thus luminescence properties, vary across a broad range of excitation power densities (10^1 to 10^6 W/cm^2) and dopant concentrations. This suggests several guidelines for choosing the proper excitation power for given application. For photophysical characterization, TRPL measurements should be acquired at a range of powers (e.g., 10^2-10^5 W/cm^2 for single UCNPs or 1-100 W/cm^2 for ensembles) to document the power dependence. Mechanistic conclusions should be drawn only after holistic photophysical modeling that incorporates orthogonal techniques. To ensure reproducibility in ET-based biological assays and imaging methods that use lifetimes for contrast, such measurements should be conducted at the lowest possible excitation fluences, particularly for high dopant concentrations. The unique power-dependence of UCNP lifetimes indicate that higher powers can be used to decrease τ_{eff} to increase maximum scan rate or modulation frequency for applications such as scanning microscopy.[61]
2. *In UCNPs, the actual lifetime of a unit of excitation energy is much shorter than the observed luminescence decay lifetime*. Individual dopant ions in UCNPs cycle among their $4f^N$ excited states on time scales an order of magnitude faster than τ_{eff}. This suggests that the optical properties of nanoparticles may be further engineered to modulate at frequencies much faster than τ_{eff}, which would be attractive for applications such as scanning and super-resolution microscopy, where the long luminescence lifetime of UCNPs limits throughput and resolution.[61]
3. *Energy transfer in UCNPs is dependent on a complex system of photophysical interactions.* Similar to biological networks, the behavior of these networks cannot be understood by analyzing individual transitions. Instead, such complex networks must be investigated holistically, aided by careful modeling, high-throughput screening, data mining, and multivariate analysis of many configurations, as we have shown here. Although the networks are complex, the analysis shown here (e.g., transition knockouts) is readily automated. Finally, we take inspiration in the fact that non-linear biological networks can precisely regulate transient processes[56] and also produce spontaneous patterning of complex structures.[62-64] Thus, our ability to understand and manipulate the complex ET networks in UCNPs and other multi-level optical materials[65-70] should lead to unique opportunities for patterning light emission across time and space.

Acknowledgments. A.T. was supported by the Weizmann Institute of Science - National Postdoctoral Award Program for Advancing Women in Science. B.T. was supported by a China Scholarship Council fellowship. A.C.G. was supported by a SULI internship. This work was performed at the Molecular Foundry and was supported by the Office of Science, Office of Basic Energy Sciences, of the U.S. Department of Energy under Contract No. DE-AC02-05CH11231.

Supporting information available. Additional experimental and theoretical methods, emission spectra, simulated lifetime traces, and knockout interaction analysis. This information is available free of charge *via* the Internet at http://pubs.acs.org.

References

1. Wilhelm, S., Perspectives for Upconverting Nanoparticles. *ACS Nano* **2017**, *11*, 10644-10653.
2. Zhou, B.; Shi, B.; Jin, D.; Liu, X., Controlling Upconversion Nanocrystals for Emerging Applications. *Nat. Nanotechnol.* **2015**, *10*, 924.
3. Chan, E. M., Combinatorial Approaches for Developing Upconverting Nanomaterials: High-Throughput Screening, Modeling, and Applications. *Chem. Soc. Rev.* **2015**, *44*, 1653-1679.
4. Nam, S. H.; Bae, Y. M.; Park, Y. I.; Kim, J. H.; Kim, H. M.; Choi, J. S.; Lee, K. T.; Hyeon, T.; Suh, Y. D., Long-Term Real-Time Tracking of Lanthanide Ion Doped Upconverting Nanoparticles in Living Cells. *Angew. Chem.* **2011**, *123*, 6217-6221.
5. Levy, E. S.; Tajon, C. A.; Bischof, T. S.; Iafrati, J.; Fernandez-Bravo, A.; Garfield, D. J.; Chamanzar, M.; Maharbiz, M. M.; Sohal, V. S.; Schuck, P. J., et al., Energy-Looping Nanoparticles: Harnessing Excited-State Absorption for Deep-Tissue Imaging. *ACS Nano* **2016**, *10*, 8423-8433.
6. Wu, S.; Han, G.; Milliron, D. J.; Aloni, S.; Altoe, V.; Talapin, D. V.; Cohen, B. E.; Schuck, P. J., Non-Blinking and Photostable Upconverted Luminescence from Single Lanthanide-Doped Nanocrystals. *Proc. Natl. Acad. Sci. U. S. A.* **2009**, *106*, 10917.
7. Chen, S.; Weitemier, A. Z.; Zeng, X.; He, L.; Wang, X.; Tao, Y.; Huang, A. J. Y.; Hashimotodani, Y.; Kano, M.; Iwasaki, H., et al., Near-Infrared Deep Brain Stimulation Via Upconversion Nanoparticle–Mediated Optogenetics. *Science* **2018**, *359*, 679.
8. Wu, X.; Zhang, Y.; Takle, K.; Bilsel, O.; Li, Z.; Lee, H.; Zhang, Z.; Li, D.; Fan, W.; Duan, C., et al., Dye-Sensitized Core/Active Shell Upconversion Nanoparticles for Optogenetics and Bioimaging Applications. *ACS Nano* **2016**, *10*, 1060-1066.
9. Idris, N. M.; Gnanasammandhan, M. K.; Zhang, J.; Ho, P. C.; Mahendran, R.; Zhang, Y., In Vivo Photodynamic Therapy Using Upconversion Nanoparticles as Remote-Controlled Nanotransducers. *Nat. Med.* **2012**, *18*, 1580.
10. Liu, Y.; Lu, Y.; Yang, X.; Zheng, X.; Wen, S.; Wang, F.; Vidal, X.; Zhao, J.; Liu, D.; Zhou, Z., et al., Amplified Stimulated Emission in Upconversion Nanoparticles for Super-Resolution Nanoscopy. *Nature* **2017**, *543*, 229.
11. Chen, G.; Shen, J.; Ohulchanskyy, T. Y.; Patel, N. J.; Kutikov, A.; Li, Z.; Song, J.; Pandey, R. K.; Ågren, H.; Prasad, P. N., et al., (A-Naybf4:Tm3+)/Caf2 Core/Shell Nanoparticles with Efficient

near-Infrared to near-Infrared Upconversion for High-Contrast Deep Tissue Bioimaging. *ACS Nano* **2012**, *6*, 8280-8287.
12. Chen, C.; Wang, F.; Wen, S.; Su, Q. P.; Wu, M. C. L.; Liu, Y.; Wang, B.; Li, D.; Shan, X.; Kianinia, M., et al., Multi-Photon near-Infrared Emission Saturation Nanoscopy Using Upconversion Nanoparticles. *Nat. Commun.* **2018**, *9*, 3290.
13. Tian, B.; Fernandez-Bravo, A.; Najafiaghdam, H.; Torquato, N. A.; Altoe, M. V. P.; Teitelboim, A.; Tajon, C. A.; Tian, Y.; Borys, N. J.; Barnard, E. S., et al., Low Irradiance Multiphoton Imaging with Alloyed Lanthanide Nanocrystals. *Nat. Commun.* **2018**, *9*, 3082.
14. Liu, Q.; Zhang, Y.; Peng, C. S.; Yang, T.; Joubert, L.-M.; Chu, S., Single Upconversion Nanoparticle Imaging at Sub-10 W Cm−2 Irradiance. *Nat. Photonics* **2018**, *12*, 548-553.
15. Rodríguez-Sevilla, P.; Zhang, Y.; Haro-González, P.; Sanz-Rodríguez, F.; Jaque, F.; Solé, J. G.; Liu, X.; Jaque, D., Thermal Scanning at the Cellular Level by an Optically Trapped Upconverting Fluorescent Particle. *Adv. Mater.* **2016**, *28*, 2421-2426.
16. Kilbane, J. D.; Chan, E. M.; Monachon, C.; Borys, N. J.; Levy, E. S.; Pickel, A. D.; Urban, J. J.; Schuck, P. J.; Dames, C., Far-Field Optical Nanothermometry Using Individual Sub-50 Nm Upconverting Nanoparticles. *Nanoscale* **2016**, *8*, 11611-11616.
17. Rodríguez-Sevilla, P.; Zhang, Y.; de Sousa, N.; Marqués, M. I.; Sanz-Rodríguez, F.; Jaque, D.; Liu, X.; Haro-González, P., Optical Torques on Upconverting Particles for Intracellular Microrheometry. *Nano Lett.* **2016**, *16*, 8005-8014.
18. Lu, Y.; Zhao, J.; Zhang, R.; Liu, Y.; Liu, D.; Goldys, E. M.; Yang, X.; Xi, P.; Sunna, A.; Lu, J., et al., Tunable Lifetime Multiplexing Using Luminescent Nanocrystals. *Nat. Photonics* **2013**, *8*, 32.
19. Deng, R.; Qin, F.; Chen, R.; Huang, W.; Hong, M.; Liu, X., Temporal Full-Colour Tuning through Non-Steady-State Upconversion. *Nat. Nanotechnol.* **2015**, *10*, 237.
20. Fernandez-Bravo, A.; Yao, K.; Barnard, E. S.; Borys, N. J.; Levy, E. S.; Tian, B.; Tajon, C. A.; Moretti, L.; Altoe, M. V.; Aloni, S., et al., Continuous-Wave Upconverting Nanoparticle Microlasers. *Nat. Nanotechnol.* **2018**, *13*, 572–577.
21. Fisher, J.; Zhao, B.; Lin, C.; Berry, M.; May, P. S.; Smith, S., Spectroscopic Imaging and Power Dependence of near-Infrared to Visible Upconversion Luminescence from Nayf4:Yb3+,Er3+ Nanoparticles on Nanocavity Arrays. *J. Phys. Chem. C* **2015**, *119*, 24976-24982.
22. LaBoda, C. D.; Dwyer, C. L., Upconverting Nanoparticle Relays for Resonance Energy Transfer Networks. *Adv. Funct. Mater.* **2016**, *26*, 2866-2874.
23. Goldschmidt, J. C.; Fischer, S., Upconversion for Photovoltaics – a Review of Materials, Devices and Concepts for Performance Enhancement. *Adv. Opt. Mater.* **2015**, *3*, 510-535.
24. Chan, E. M.; Levy, E. S.; Cohen, B. E., Rationally Designed Energy Transfer in Upconverting Nanoparticles. *Adv. Mater.* **2015**, *27*, 5753-5761.
25. Chan, E. M.; Gargas, D. J.; Schuck, P. J.; Milliron, D. J., Concentrating and Recycling Energy in Lanthanide Codopants for Efficient and Spectrally Pure Emission: The Case of Nayf4:Er3+/Tm3+ Upconverting Nanocrystals. *J. Phys. Chem. B* **2012**, *116*, 10561-10570.
26. Buckhout-White, S.; Spillmann, C. M.; Algar, W. R.; Khachatrian, A.; Melinger, J. S.; Goldman, E. R.; Ancona, M. G.; Medintz, I. L., Assembling Programmable Fret-Based Photonic Networks Using Designer DNA Scaffolds. *Nat. Commun.* **2014**, *5*, 5615.
27. Şener, M. K.; Park, S.; Lu, D.; Damjanović, A.; Ritz, T.; Fromme, P.; Schulten, K., Excitation Migration in Trimeric Cyanobacterial Photosystem I. *J. Chem. Phys.* **2004**, *120*, 11183-11195.

28. Pistol, C.; Dwyer, C.; Lebeck, A. R., Nanoscale Optical Computing Using Resonance Energy Transfer Logic. *IEEE Micro* **2008**, *28*, 7-18.
29. Nellore, V.; Xi, S.; Dwyer, C., Self-Assembled Resonance Energy Transfer Keys for Secure Communication over Classical Channels. *ACS Nano* **2015**, *9*, 11840-11848.
30. Naruse, M.; Aono, M.; Kim, S.-J.; Kawazoe, T.; Nomura, W.; Hori, H.; Hara, M.; Ohtsu, M., Spatiotemporal Dynamics in Optical Energy Transfer on the Nanoscale and Its Application to Constraint Satisfaction Problems. *Phys. Rev. B* **2012**, *86*, 125407.
31. Boccaletti, S.; Latora, V.; Moreno, Y.; Chavez, M.; Hwang, D. U., Complex Networks: Structure and Dynamics. *Phys. Rep.* **2006**, *424*, 175-308.
32. Wang, Y.; Tu, L.; Zhao, J.; Sun, Y.; Kong, X.; Zhang, H., Upconversion Luminescence of B-Nayf4: Yb3+, Er3+@B-Nayf4 Core/Shell Nanoparticles: Excitation Power Density and Surface Dependence. *J. Phys. Chem. C* **2009**, *113*, 7164-7169.
33. Hossan, M. Y.; Hor, A.; Luu, Q.; Smith, S. J.; May, P. S.; Berry, M. T., Explaining the Nanoscale Effect in the Upconversion Dynamics of B-Nayf4:Yb3+, Er3+ Core and Core–Shell Nanocrystals. *J. Phys. Chem. C* **2017**, *121*, 16592-16606.
34. Zhao, J.; Lu, Z.; Yin, Y.; McRae, C.; Piper, J. A.; Dawes, J. M.; Jin, D.; Goldys, E. M., Upconversion Luminescence with Tunable Lifetime in Nayf4:Yb,Er Nanocrystals: Role of Nanocrystal Size. *Nanoscale* **2013**, *5*, 944-952.
35. Wang, Y.; Deng, R.; Xie, X.; Huang, L.; Liu, X., Nonlinear Spectral and Lifetime Management in Upconversion Nanoparticles by Controlling Energy Distribution. *Nanoscale* **2016**, *8*, 6666-6673.
36. Anderson, R. B.; Smith, S. J.; May, P. S.; Berry, M. T., Revisiting the Nir-to-Visible Upconversion Mechanism in B-Nayf4:Yb3+,Er3+. *J. Phys. Chem. Lett.* **2014**, *5*, 36-42.
37. Savchuk, O. A.; Haro-González, P.; Carvajal, J. J.; Jaque, D.; Massons, J.; Aguiló, M.; Díaz, F., Er:Yb:Nay2f5o up-Converting Nanoparticles for Sub-Tissue Fluorescence Lifetime Thermal Sensing. *Nanoscale* **2014**, *6*, 9727-9733.
38. Pickel, A. D.; Teitelboim, A.; Chan, E. M.; Borys, N. J.; Schuck, P. J.; Dames, C., Apparent Self-Heating of Individual Upconverting Nanoparticle Thermometers. *Nat. Commun.* **2018**, *9*, 4907.
39. Garfield, D. J.; Borys, N. J.; Hamed, S. M.; Torquato, N. A.; Tajon, C. A.; Tian, B.; Shevitski, B.; Barnard, E. S.; Suh, Y. D.; Aloni, S., et al., Enrichment of Molecular Antenna Triplets Amplifies Upconverting Nanoparticle Emission. *Nat. Photonics* **2018**.
40. Johnson, N. J. J.; He, S.; Diao, S.; Chan, E. M.; Dai, H.; Almutairi, A., Direct Evidence for Coupled Surface and Concentration Quenching Dynamics in Lanthanide-Doped Nanocrystals. *J. Am. Chem. Soc.* **2017**, *139*, 3275-3282.
41. Gargas, D. J.; Chan, E. M.; Ostrowski, A. D.; Aloni, S.; Altoe, M. V. P.; Barnard, E. S.; Sanii, B.; Urban, J. J.; Milliron, D. J.; Cohen, B. E., et al., Engineering Bright Sub-10-Nm Upconverting Nanocrystals for Single-Molecule Imaging. *Nat. Nanotechnol.* **2014**, *9*, 300.
42. Fischer, S.; Bronstein, N. D.; Swabeck, J. K.; Chan, E. M.; Alivisatos, A. P., Precise Tuning of Surface Quenching for Luminescence Enhancement in Core–Shell Lanthanide-Doped Nanocrystals. *Nano Lett.* **2016**, *16*, 7241-7247.
43. Zuo, J.; Sun, D.; Tu, L.; Wu, Y.; Cao, Y.; Xue, B.; Zhang, Y.; Chang, Y.; Liu, X.; Kong, X., et al., Precisely Tailoring Upconversion Dynamics Via Energy Migration in Core–Shell Nanostructures. *Angew. Chem. Int. Ed.* **2018**, *57*, 3054-3058.

44. Chen, G.; Qiu, H.; Prasad, P. N.; Chen, X., Upconversion Nanoparticles: Design, Nanochemistry, and Applications in Theranostics. *Chem. Rev.* **2014**, *114*, 5161-5214.
45. Yao, C.; Wang, P.; Li, X.; Hu, X.; Hou, J.; Wang, L.; Zhang, F., Near‐Infrared‐Triggered Azobenzene‐Liposome/Upconversion Nanoparticle Hybrid Vesicles for Remotely Controlled Drug Delivery to Overcome Cancer Multidrug Resistance. *Adv. Mater.* **2016**, *28*, 9341-9348.
46. Zhan, Q.; Liu, H.; Wang, B.; Wu, Q.; Pu, R.; Zhou, C.; Huang, B.; Peng, X.; Ågren, H.; He, S., Achieving High-Efficiency Emission Depletion Nanoscopy by Employing Cross Relaxation in Upconversion Nanoparticles. *Nat. Commun.* **2017**, *8*, 1058.
47. Berezin, M. Y.; Achilefu, S., Fluorescence Lifetime Measurements and Biological Imaging. *Chem. Rev.* **2010**, *110*, 2641-2684.
48. Liu, G.; Jacquier, B., *Spectroscopic Properties of Rare Earths in Optical Materials*; Springer: Berlin, 2005.
49. Strogatz, S. H., Exploring Complex Networks. *Nature* **2001**, *410*, 268.
50. Gordon, D. M., The Ecology of Collective Behavior. *PLoS Biol.* **2014**, *12*, e1001805.
51. Cilliers, P., *Complexity and Postmodernism*; Routledge: London, 2002, p 3.
52. Ostrowski, A. D.; Chan, E. M.; Gargas, D. J.; Katz, E. M.; Han, G.; Schuck, P. J.; Milliron, D. J.; Cohen, B. E., Controlled Synthesis and Single-Particle Imaging of Bright, Sub-10 Nm Lanthanide-Doped Upconverting Nanocrystals. *ACS Nano* **2012**, *6*, 2686-2692.
53. Li, X.; Shen, D.; Yang, J.; Yao, C.; Che, R.; Zhang, F.; Zhao, D., Successive Layer-by-Layer Strategy for Multi-Shell Epitaxial Growth: Shell Thickness and Doping Position Dependence in Upconverting Optical Properties. *Chem. Mater.* **2013**, *25*, 106-112.
54. Walsh, B. M., Judd-Ofelt Theory: Principles and Practices. In *Advances in Spectroscopy for Lasers and Sensing*, Springer: 2006; pp 403-433.
55. Kushida, T., Energy Transfer and Cooperative Optical Transitions in Rare-Earth Doped Inorganic Materials. I. Transition Probability Calculation. *J. Phys. Soc. Jpn.* **1973**, *34*, 1318-1326.
56. Gillespie, D. T., Exact Stochastic Simulation of Coupled Chemical Reactions. *J. Phys. Chem.* **1977**, *81*, 2340-2361.
57. Ledoux, G.; Amans, D.; Joubert, M. F.; Mahler, B.; Mishra, S.; Daniele, S.; Dujardin, C., Modeling Energy Migration for Upconversion Materials. *J. Phys. Chem. C* **2018**, *122*, 888-893.
58. Dukhno, O.; Przybilla, F.; Collot, M.; Klymchenko, A.; Pivovarenko, V.; Buchner, M.; Muhr, V.; Hirsch, T.; Mely, Y., Quantitative Assessment of Energy Transfer in Upconverting Nanoparticles Grafted with Organic Dyes. *Nanoscale* **2017**, *9*, 11994-12004.
59. Melton David, W., Gene Targeting in the Mouse. *Bioessays* **1994**, *16*, 633-638.
60. Semenov, S. N.; Kraft, L. J.; Ainla, A.; Zhao, M.; Baghbanzadeh, M.; Campbell, V. E.; Kang, K.; Fox, J. M.; Whitesides, G. M., Autocatalytic, Bistable, Oscillatory Networks of Biologically Relevant Organic Reactions. *Nature* **2016**, *537*, 656.
61. Pichaandi, J.; Boyer, J.-C.; Delaney, K. R.; van Veggel, F. C. J. M., Two-Photon Upconversion Laser (Scanning and Wide-Field) Microscopy Using Ln3+-Doped Nayf4 Upconverting Nanocrystals: A Critical Evaluation of Their Performance and Potential in Bioimaging. *J. Phys. Chem. C* **2011**, *115*, 19054-19064.
62. Tompkins, N.; Li, N.; Girabawe, C.; Heymann, M.; Ermentrout, G. B.; Epstein, I. R.; Fraden, S., Testing Turing's Theory of Morphogenesis in Chemical Cells. *Proc. Natl. Acad. Sci. U. S. A.* **2014**, *111*, 4397.

63. Müller, P.; Rogers, K. W.; Jordan, B. M.; Lee, J. S.; Robson, D.; Ramanathan, S.; Schier, A. F., Differential Diffusivity of Nodal and Lefty Underlies a Reaction-Diffusion Patterning System. *Science* **2012**, *336*, 721.
64. Meinhardt, H., Models of Biological Pattern Formation: From Elementary Steps to the Organization of Embryonic Axes. In *Current Topics in Developmental Biology*, Schnell, S.; Maini, P. K.; Newman, S. A.; Newman, T. J., Eds. Academic Press: 2008; Vol. 81, pp 1-63.
65. Teitelboim, A.; Meir, N.; Kazes, M.; Oron, D., Colloidal Double Quantum Dots. *Acc. Chem. Res.* **2016**, *49*, 902-910.
66. Vörös, M.; Galli, G.; Zimanyi, G. T., Colloidal Nanoparticles for Intermediate Band Solar Cells. *ACS Nano* **2015**, *9*, 6882-6890.
67. Ghosh, A.; Isbaner, S.; Veiga-Gutiérrez, M.; Gregor, I.; Enderlein, J.; Karedla, N., Quantifying Microsecond Transition Times Using Fluorescence Lifetime Correlation Spectroscopy. *J. Phys. Chem. Lett.* **2017**, *8*, 6022-6028.
68. Fisher, B. R.; Eisler, H.-J.; Stott, N. E.; Bawendi, M. G., Emission Intensity Dependence and Single-Exponential Behavior in Single Colloidal Quantum Dot Fluorescence Lifetimes. *J. Phys. Chem. B* **2004**, *108*, 143-148.
69. Murotani, H.; Yamada, Y.; Honda, Y.; Amano, H., Excitation Density Dependence of Radiative and Nonradiative Recombination Lifetimes in Ingan/Gan Multiple Quantum Wells. *physica status solidi (b)* **2014**, *252*, 940-945.
70. McCusker, C. E.; Castellano, F. N., Materials Integrating Photochemical Upconversion. *Top. Curr. Chem.* **2016**, *374*, 19.

TOC Graphic

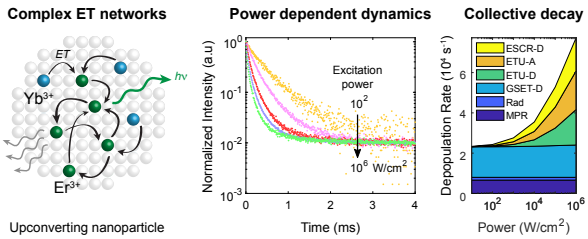
Complex ET networks
Power dependent dynamics
Collective decay
ET
hν
Yb3+
Er3+
Upconverting nanoparticle
Normalized Intensity (a.u)
Excitation power
10^2
10^6 W/cm^2
Time (ms)
Depopulation Rate (10^4 s^-1)
ESCR-D
ETU-A
ETU-D
GSET-D
Rad
MPR
Power (W/cm^2)